Enhanced Thermoelectric Performance of Ba8Ga16Ge30 Clathrate by Modulation Doping and Improved Carrier Mobility

ADVANCED ELECTRONIC MATERIALS
www.advelectronicmat.de

Enhanced Thermoelectric Performance of $Ba_8Ga_{16}Ge_{30}$ Clathrate by Modulation Doping and Improved Carrier Mobility

*Yifei Zhang, Joakim Brorsson, Ren Qiu, and Anders E. C. Palmqvist**

Type-I inorganic clathrates are promising high temperature thermoelectric materials. They are known for their intrinsic low thermal conductivity, but a moderate power factor leaves room for further improvement. In this paper, a new route for improving the power factor by enhanced carrier mobility achieved via modulation doping is reported. A series of clathrates with composition $Ba_8(Al_xGa_{1-x})_{16}Ge_{30}$ are synthesized through ball milling and spark plasma sintering of mixtures of $Ba_8Al_{16}Ge_{30}$ and $Ba_8Ga_{16}Ge_{30}$. Among the materials with $x = 0.20$, 0.23, and 0.25, it is found that the electrical conductivity is significantly enhanced with increasing x, while the Seebeck coefficient decreases slightly. It is further revealed that the carrier mobility of the sintered sample $x = 0.25$ is greatly increased, reaching a value that exceeds that for a single crystal. Electron microscopy analysis reveals that the material consists of a heterostructure and is composed of a Ga-rich clathrate matrix phase and Al particles, suggesting that the power factor enhancement is due to modulation doping. As a result, the highest power factor is achieved for $Ba_8(Al_{0.25}Ga_{0.75})_{16}Ge_{30}$, with a value of 1.89 mW m^{-1} K^{-2} at 800 °C. Consequently, the maximum zT of sample $x = 0.25$ reaches 0.93 at 800 °C.

1. Introduction

The thermoelectric effect describes the coupling between a thermal and a potential gradient and can be exploited for electrical energy generation.[1–4] The thermodynamic efficiency of thermoelectric energy conversion scales with the dimensionless quantity zT, which is defined as

$$zT = \frac{S^2\sigma}{\kappa} \cdot T = \frac{S^2\sigma}{\kappa_e + \kappa_l} \cdot T \quad (1)$$

This so-called thermoelectric figure of merit comprises three temperature-dependent materials properties. The Seebeck coefficient S is a measure of the strength of the coupling between the thermal and potential gradients, whereas σ and κ denote electrical and thermal conductivity, respectively. The thermal conductivity comprises both electronic κ_e and phononic (lattice) κ_l contributions. The former term is proportional to the electrical conductivity σ according to Wiedemann–Franz law.

Inorganic clathrates are promising high temperature thermoelectric materials. They can be regarded as realizations of the phonon-glass electron-crystal concept, combining relatively large electrical conductivity (electron crystal) with very low thermal conductivity (phonon glass).[5] These materials are usually covalently bonded semiconductors with relatively small band gaps and typically comprise elements from groups 13, 14, and 15 of the periodic table.[6] $Ba_8Ga_{16}Ge_{30}$ is one of the most studied clathrates and shows the most promising thermoelectric performance. A single crystal of $Ba_8Ga_{16}Ge_{30}$ grown by the Czochralski method was found to exhibit a record high zT of 1.35 at 630 °C.[7] Nevertheless, zT values of polycrystalline clathrate compounds rarely exceeds 1, and for instance a zT of 0.86 at 670 °C was obtained for polycrystalline $Ba_8Ga_{16}Ge_{30}$.[8]

From a fundamental materials science perspective, there is a conflict between simultaneously enhancing the electrical conductivity and the Seebeck coefficient, since these two parameters have an opposing dependence on the charge carrier concentration and mobility.[9] There exists strategies to enhance the Seebeck coefficient solely, mainly by manipulating the band structure near the Fermi level, for instance through resonant states and band convergence.[10,11] Yet, this requires knowledge of the band structure and is only feasible for certain materials systems. An alternative way to overcome the intercorrelation

Y. Zhang, J. Brorsson, Prof. A. E. C. Palmqvist
Department of Chemistry and Chemical Engineering
Chalmers University of Technology
Gothenburg SE-41296, Sweden
R. Qiu
Department of Physics
Chalmers University of Technology
Gothenburg SE-41296, Sweden
E-mail: anders.palmqvist@chalmers.se
The ORCID identification number(s) for the author(s) of this article can be found under https://doi.org/10.1002/aelm.202000782.

DOI: 10.1002/aelm.202000782

between electrical conductivity and Seebeck coefficient is through modulation doping. Zebarjadi et al. were among the first to employ modulation doping in SiGe alloys, and afterward this method was applied to other systems, such as BiAgSeS, BiCuSeO, PbTe, and $SrTiO_3$.[12–16] Heterostructures are usually created in modulation doped materials, which are composed of an undoped matrix phase and a doped phase. Charge carriers can become separated from the latter and transferred to the former. Because of the absence of impurity scattering, these charge carriers move faster in the undoped matrix. As a result, the electrical conductivity can be enhanced without decreasing the Seebeck coefficient.

Most previous clathrate studies have focused on synthesizing homogeneous compounds; wherein, accordingly, improvements of electrical conductivity are always counteracted by a decrease of the Seebeck coefficient, or the vice versa. Recently, transition metal element containing clathrates have been widely investigated.[17–20] A large figure of merit $zT = 0.9$ at 630 °C was found for a single crystal $Ba_8Cu_{4.4}Ga_{1.0}Ge_{40.4}$.[20] The high zT, which was mainly attributed to the suppression of vacancies that, in turn, increases the charge carrier mobility drastically. A zT value of 1.2 at 730 °C was achieved for polycrystalline $Ba_8Ni_{0.31}Zn_{0.52}Ga_{13.06}Ge_{32.2}$ by cross-substitution of the host elements.[21]

In this paper, we explore the concept of modulation doping in clathrates, by alloying $Ba_8Ga_{16}Ge_{30}$ and $Ba_8Al_{16}Ge_{30}$ via ball milling and spark plasma sintering and forming a series of clathrates with composition $Ba_8(Al_xGa_{1-x})_{16}Ge_{30}$. The thermoelectric properties of the materials were measured and found to depend largely on the value of x. Electron microscopy analysis was employed to study the effect of the alloying on the microstructure of the materials and to correlate it to their thermal transport properties.

2. Results and Discussion

2.1. Electrical Transport Properties

The electrical transport properties of $Ba_8(Al_xGa_{1-x})_{16}Ge_{30}$ (x = 0, 0.20, 0.23, 0.25, 0.33, 0.50, and 1) are shown in **Figure 1**a,b. All samples have negative Seebeck coefficient and thus demonstrate an n-type semiconductor behavior. $Ba_8Al_{16}Ge_{30}$ (x = 1) and $Ba_8Ga_{16}Ge_{30}$ (x = 0) display transport properties that are consistent with those reported earlier.[8,22,23] The high absolute Seebeck coefficient and resistivity indicates that the $Ba_8Ga_{16}Ge_{30}$ material is only slightly doped and has a relatively low carrier concentration. Due to the bipolar effect, both the absolute Seebeck coefficient and the electrical resistivity of $Ba_8Ga_{16}Ge_{30}$ decrease above 550 °C. On the other hand, $Ba_8Al_{16}Ge_{30}$ shows a typical metallic behavior, as is indicated by the fact that the resistivity increases with temperature while the Seebeck coefficient reaches only –14 μV K^{-1} at 100 °C.

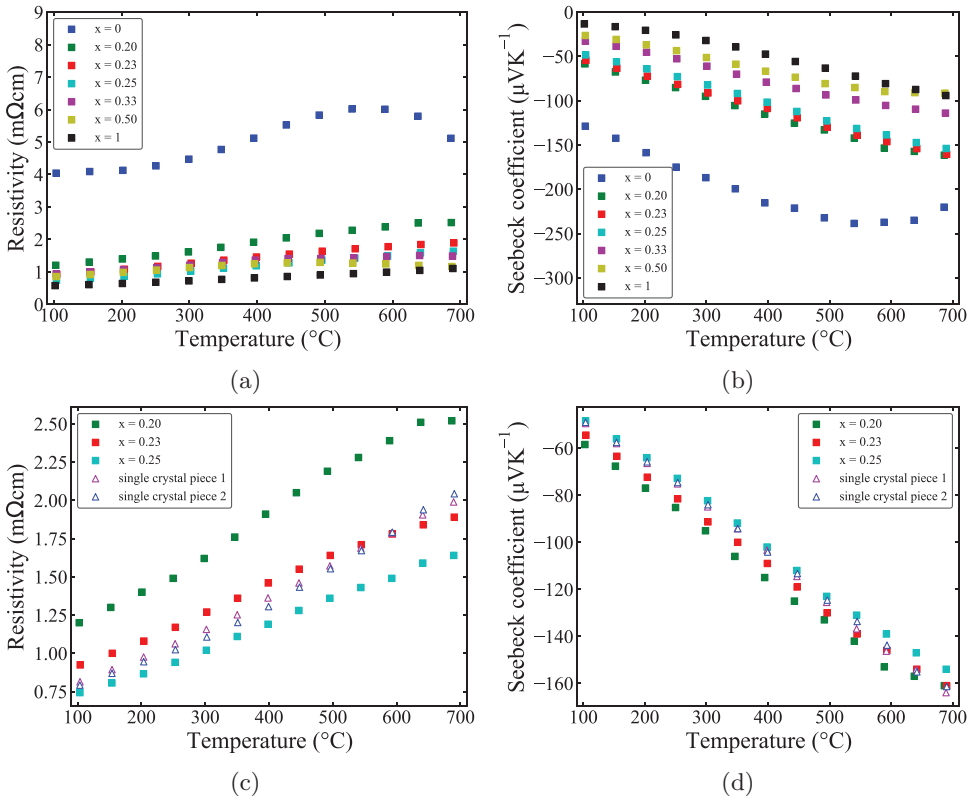

Figure 1. a,c) Electrical resistivity and b,d) Seebeck coefficient of $Ba_8(Al_xGa_{1-x})_{16}Ge_{30}$ materials pressed into pellets by SPS, which in (c) and (d) are compared to the properties of two sections from a Czochralski-grown $Ba_8(Al_{0.25}Ga_{0.75})_{16}Ge_{30}$ single crystal.

Gradually increasing the amount of $Ba_8Al_{16}Ge_{30}$ in the matrix of $Ba_8Ga_{16}Ge_{30}$, decreases the resistivity and the absolute value of the Seebeck coefficient. The absolute value of the maximum Seebeck coefficient decreases from −238 μV K^{-1} (x = 0) to −114 μV K^{-1} (x = 0.33). The data indicates that the degree of doping has reached a level that is considered heavily doped already for the sample with the composition of x = 0.33. For the sample with x = 0.50, the Seebeck coefficient reaches a plateau at 550 °C, meanwhile the resistivity decreases gradually. Such a behavior can be explained by the bipolar effect in $Ba_8Ga_{16}Ge_{30}$, which occurs at 550 °C. As shown in Figure S1, (Supporting Information) this sample contains many impurity phases, including undoped $Ba_8Ga_{16}Ge_{30}$ and elemental Al.

By tuning the doping level slightly ($0.20 \le x \le 0.25$), the resistivity can be further decreased, achieving ≈30 % reduction in the whole temperature range from 100–700 °C. Meanwhile, the reduction of absolute Seebeck coefficient is not that large, decreasing only slightly from −161 μV K^{-1} (x = 0.20) to −154 μV K^{-1} (x = 0.25) at 700 °C. In general, alloying (or doping) a semiconducting matrix phase homogeneously with a metallic phase has a positive impact on the electrical conductivity, by increasing the carrier concentration. However, the charge carrier mobility is usually reduced due to the ionized impurity scattering, hence decreasing the absolute value of the Seebeck coefficient. Conversely, our $Ba_8(Al_xGa_{1-x})_{16}Ge_{30}$ (x = 0.23 and 0.25) samples show an improved electrical conductivity without the corresponding decrease in the Seebeck coefficient, which is suggested to result from modulation doping.

To confirm this idea, the transport properties of the SPS sintered samples are compared with those of a reference single crystal. The single crystal was grown by the Czochralski method with the composition $Ba_8(Al_{0.25}Ga_{0.75})_{16}Ge_{30}$; more details about the single crystal will be published in a separate study. As is shown in Figure 1c,d, the single crystal samples exhibit similar Seebeck coefficient as the sintered sample x = 0.25, indicating that the band structures of these samples are consistent. In contrast, the sintered sample with x = 0.25 has a lower resistivity than the single crystal in the entire temperature range studied and this is also true for the sintered sample with x = 0.23 above 600 °C. The similar values of the Seebeck coefficient indicate that the carrier mobility of the sintered samples is not lower than that of the single crystal. Therefore, the improved resistivity and nearly unchanged Seebeck coefficient strongly supports the idea that our sintered samples (x = 0.23 and 0.25) are modulation doped.

In order to further illustrate the origin of the improved transport properties, the charge carrier mobility needs to be examined in more depth. To this end, Snyder et al. very recently proposed the weighted mobility μ_w, which can be calculated as

$$\mu_w = 331\frac{\mathrm{cm}^2}{\mathrm{Vs}}\left(\frac{\mathrm{m\Omega\,cm}}{\rho}\right)\left(\frac{T}{300\ \mathrm{K}}\right)^{-3/2}\left[\frac{\exp\left[\frac{|S|}{k_B/e}-2\right]}{1+\exp\left[-5\left(\frac{|S|}{k_B/e}-1\right)\right]}+\frac{\frac{3}{\pi^2}\frac{|S|}{k_B/e}}{1+\exp\left[5\frac{|S|}{k_B/e}-1\right]}\right] \quad (2)$$

where k_B is the Boltzmann constant and e is the elementary charge, while ρ and T refer to the resistivity and absolute temperature, respectively.[24] Consequently, the weighted mobility can be calculated directly from the resistivity and Seebeck coefficient data and used to estimate the charge carrier mobility. As is shown in **Figure 2**a, the weighted mobility of our $Ba_8Ga_{16}Ge_{30}$ (sample x = 0) is consistent with those obtained from Hall measurements, so it is physically reasonable to use the weighted mobility for estimating the charge carrier mobility in our samples. Alloying $Ba_8Ga_{16}Ge_{30}$ with $Ba_8Al_{16}Ge_{30}$ reduces the weighted mobility, but still, the mobility of samples x = 0.23 and 0.25 is significantly higher than that of the other sintered samples. More astonishingly, the mobility of these two samples (x = 0.23 and 0.25) is comparable and even higher than that of the single crystal. The carrier mobility of the sintered sample should normally be lower than that of the single crystal, due to the presence of grain boundaries. However, we do not observe such behavior. Alternatively, the different mobilities between the sintered and single crystal samples could be related to the

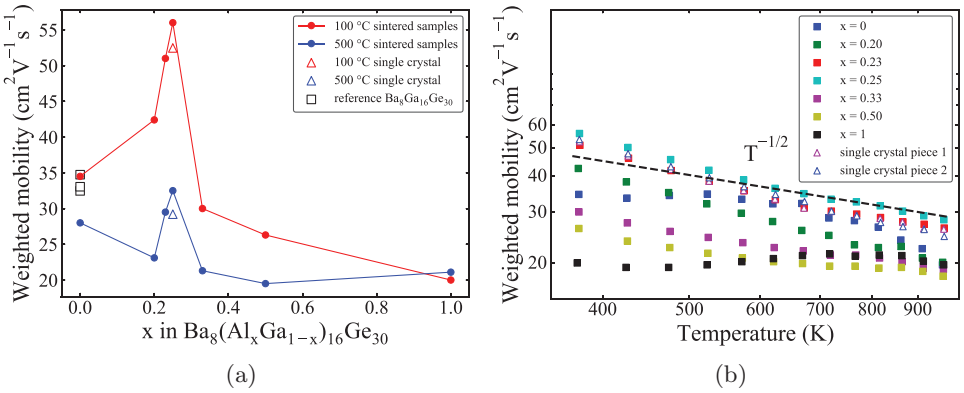

Figure 2. a) Weighted charge carrier mobility (μ_w) at 100 and 500 °C for $Ba_8(Al_xGa_{1-x})_{16}Ge_{30}$ calculated from Equation 2 for the SPS sintered samples and the single crystal. Here μ_w of the reference $Ba_8Ga_{16}Ge_{30}$ is calculated as $\mu_w \approx \mu(m^*/m_e)^{3/2}$, where μ is the drift mobility, m^* is the density of state effective mass and m_e is the electron mass, with values taken from reference.[8] b) Weighted charge carrier mobility versus absolute temperature plotted in log-log scale. The dashed line indicates the $T^{-1/2}$ temperature dependence of μ_w.

distribution of impurities, where in the sintered samples impurities could diffuse to the grain boundaries, while in the single crystal they could be trapped during growth, resulting in lower mobility. However, we have not been able to find any experimental support for a higher concentration of impurities in the single crystal and thus rule this out as a possible explanation for the enhanced mobility of the sintered samples. Therefore, we can attribute the greatly enhanced carrier mobility in our sintered samples ($x = 0.23$ and 0.25) to modulation doping. In turn, this leads to a lower electrical resistivity while the Seebeck coefficient remains unchanged.

Moreover, alloying $Ba_8Ga_{16}Ge_{30}$ with $Ba_8Al_{16}Ge_{30}$ changes the electron scattering mechanism. For most good thermoelectric materials, charge carrier mobility decreases with temperature because the electrons are scattered by phonons.[24] Specifically, acoustic phonon scattering is the dominant scattering mechanism at high temperatures, and the mobility typically shows a $T^{-3/2}$ temperature dependence, which has, for instance, been observed for the type-I clathrate $Ba_8Ga_{16}Ge_{30}$.[8] However, alloy scattering (also called disorder scattering) seems to be dominant in our modulation doped sample $x = 0.25$ since the mobility, as is shown in Figure 2b, decreases with temperature as $T^{-1/2}$.[25] Although polar scattering also shows a $T^{-1/2}$ dependence, it is typically prominent at low carrier concentration and, hence, not relevant for our heavily doped samples. The clathrate crystal structure may, however, provide an explanation for the observed behavior. In particular, the crystal structure contains cages, which can host large guest ions such as the Ba atom in the present study, and the cages are made up of the host elements (Al, Ga, and Ge). Though the host elements share the host sites (Wyckoff sites 6*c*, 16*i*, 24*k*), they are not randomly distributed. Instead, the trivalent elements (Al and Ga) preferably occupy the 6c sites.[26] Also, the site occupancy factors for the host elements differ significantly depending on the synthesis method.[22] Therefore, it is possible that alloying $Ba_8Ga_{16}Ge_{30}$ with $Ba_8Al_{16}Ge_{30}$ induces higher disorder on the host sites, which causes alloy scattering to become the dominant scattering mechanism.

The power factor of $Ba_8(Al_xGa_{1-x})_{16}Ge_{30}$ is shown in **Figure 3**. The highest power factor is achieved for sample $x = 0.25$ with a value of 1.45 mW m^{-1} K^{-2} at 700 °C. By comparison, the power factor of $Ba_8Ga_{16}Ge_{30}$ is 0.95 mW m^{-1} K^{-2} at 700 °C, so ~50 % improvement is achieved. The resistivity and Seebeck coefficient of samples $x = 0.23$ and 0.25 were additionally measured up to 850 °C, as shown in **Figure 4**. Overall the results are consistent with the previous measurements that ended at 700 °C; the standard deviation is 7 % for the resistivity and 4 % for the Seebeck coefficient, within the uncertainty of the ZEM3 instrument (10 %).[27] The materials are perhaps not completely stable up to 850 °C, because there is a deviation between the transport properties measured during the heating and cooling cycle, respectively. Nonetheless, the power factor of the samples $x = 0.23$ and 0.25 further increases to 1.82 and 1.89 mW m^{-1} K^{-2} at 800 °C, respectively. To the best of our knowledge, these values are the highest reported among polycrystalline type-I clathrate compounds, and are close to the single crystal $Ba_8Ga_{16}Ge_{30}$.[7,8,18,21,28,29]

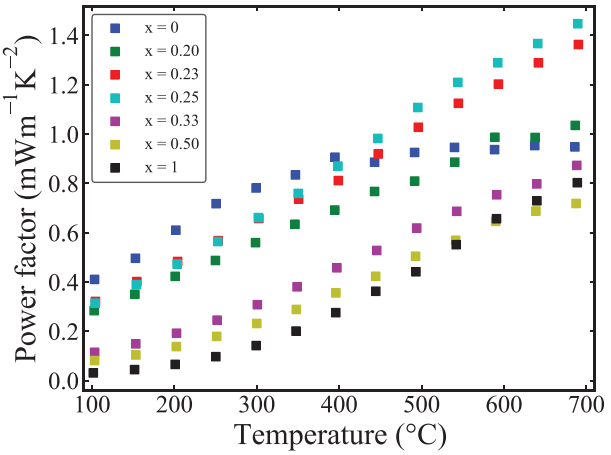

Figure 3. Power factor of $Ba_8(Al_xGa_{1-x})_{16}Ge_{30}$ materials pressed into pellets by SPS.

2.2. Microstructure Analysis

According to the XRD patterns for samples $x = 0$, 0.25 and 1, shown in **Figure 5**, they all exhibit a typical type-I clathrate structure. The impurity peak observed for sample $x = 0$ is indexed as the (111) plane of Ge, which is a common impurity for Ge-based clathrate compounds. From the peak shift, one can tell that the lattice parameter of sample $x = 0.25$ is larger than that of sample $x = 0$. This means that $Ba_8(Al_{0.25}Ga_{0.75})_{16}Ge_{30}$ is produced during the sintering, since the lattice parameter of $Ba_8Al_{16}Ge_{30}$ is larger than that of $Ba_8Ga_{16}Ge_{30}$. It is also found that the positions of the main peaks are relatively close for sample $x = 0.25$ before and after sintering, as shown in Figure 5b, indicating that $Ba_8(Al_{0.25}Ga_{0.75})_{16}Ge_{30}$ is partially formed during the mechanical ball milling. The XRD analysis did not reveal the existence of any secondary phases.

The microstructure of sample $x = 0.25$ was studied using electron microscopy, as shown in **Figures 6** and **7**. The areas 1 and 2 in Figure 6 have chemical compositions around $Ba_8Al_{2.9}Ga_{12.2}Ge_{28.2}$ and $Ba_8Al_{2.4}Ga_{12.1}Ge_{28.4}$, and the areas 1 and 3 in Figure 7 have chemical compositions around $Ba_8Al_{2.9}Ga_{11.3}Ge_{28}$ and $Ba_8Al_{2.8}Ga_{11.9}Ge_{27.9}$. These measured values are very close to the composition of the clathrate compound considering the measurement accuracy. Since the composition appears consistent throughout each area, there exists no evidence of any phase separation of the quaternary $Ba_8(Al_xGa_{1-x})_{16}Ge_{30}$ within the individual grains. In addition, particles, with sizes of about a few hundred nanometers, are observed inside the grains as well as along the boundaries. Such a microstructure could potentially enhance phonon scattering, and, thus, reduce the lattice thermal conductivity.[30]

According to the Al element maps shown in both Figure 6 and Figure 7, those hundred-nanometer-sized particles are likely to consist mainly of Al. This is also confirmed by analyzing the local chemical composition of area 3 in Figure 6 and area 2 in Figure 7. As shown in Figure 7, some Al particles are partially oxidized, which may have occurred during polishing. Because the oxidization only affects the sample surface, not the whole bulk, this sample still exhibits excellent electrical conductivity. Moreover, it is evident that Al is not homogeneously distributed throughout the sintered sample, but rather appears

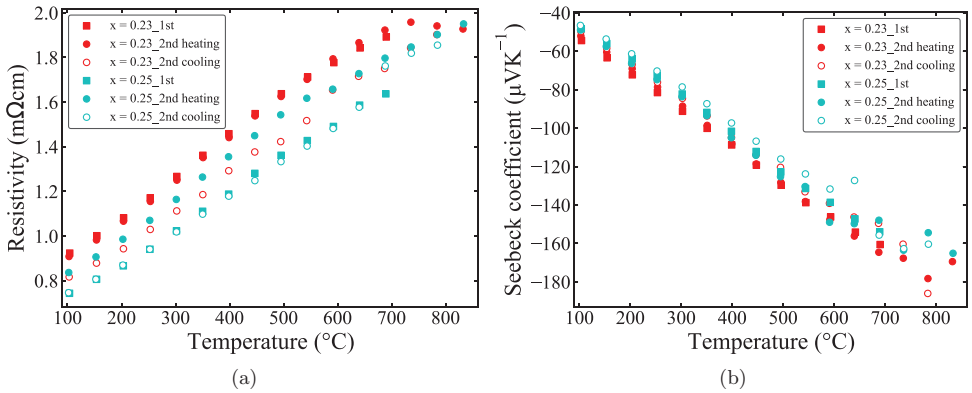

Figure 4. a) Electrical resistivity and b) Seebeck coefficient of $Ba_8(Al_xGa_{1-x})_{16}Ge_{30}$ samples $x = 0.23$ and 0.25. Here '1st' and '2nd' refer to the measurement up to 700 and 800 °C, respectively.

in higher concentrations in some areas, which include aggregation at the grain boundaries and particles inside the grains. Electron transfer from the Al particles to the main, Ga-rich, clathrate phase can be achieved without reducing the mobility significantly, which leads to an improved electrical conductivity without decreasing the Seebeck coefficient.

2.3. Thermal Conductivity

The thermal conductivity of samples x = 0, 0.20, 0.25, and 0.33 is shown in **Figure 8**a. All samples display a relatively low thermal conductivity, with the value increasing with x. As shown previously, the electrical conductivity also increases with x and the behavior of the samples change from that of a slightly doped to a heavily doped semiconductor, for which the electronic contribution (κ_e) typically dominates the thermal conductivity. Since the thermal conductivity of sample $x = 0.33$ is already too high for efficient thermoelectric conversion, the thermal conductivity was not measured for the samples with higher Al content (x = 0.5 and 1). In addition, the thermal conductivity tends to increase rapidly at high temperatures, owing to the excitation of minority charge carriers (the bipolar effect). Though the corresponding, abrupt, change appears at a lower temperature for the thermal conductivity compared to the Seebeck coefficient, this is, as has been reported previously, common for type-I clathrates.[7,31]

In order to further analyze the effect of the microstructure on the thermal conductivity, the lattice thermal conductivity is calculated using the Wiedemann–Franz law

$$\kappa_l = \kappa - \kappa_e \tag{3}$$

$$\kappa_e = L \cdot \sigma \cdot T \tag{4}$$

where the Lorenz number L is calculated from an empirical equation

$$L = 1.5 + \exp\left(-\frac{|S|}{116}\right) \tag{5}$$

which is accurate within 5 % when assuming a single parabolic band and only taking acoustic phonon scattering into account.[3,32] Although alloy scattering, rather than acoustic phonon scattering, seems to be the dominant mechanism, we still use the above formula to roughly estimate the lattice thermal conductivity.

As can be seen in Figure 8b, alloying $Ba_8Ga_{16}Ge_{30}$ with $Ba_8Al_{16}Ge_{30}$ drastically reduces the lattice thermal conductivity. The minimum lattice thermal conductivity of sample $x = 0.20$ at 600 °C is close to the theoretical limit of 0.56 W m^{-1} K^{-1} for $Ba_8Ga_{16}Ge_{30}$, represented by the dashed line in Figure 8b.

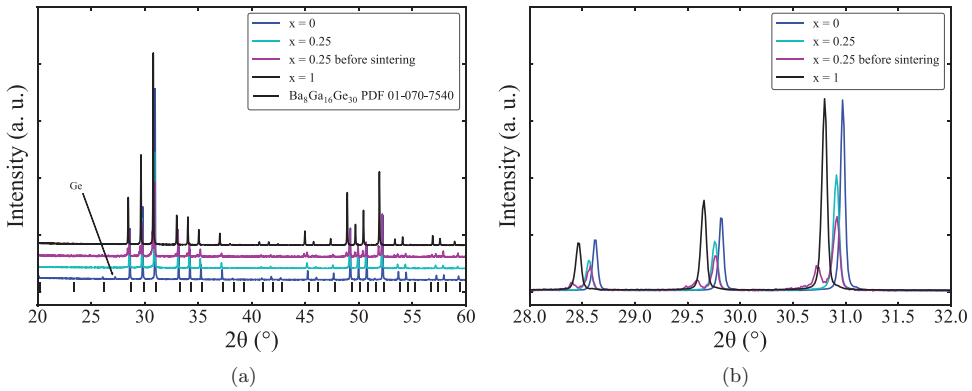

Figure 5. XRD patterns of $Ba_8(Al_xGa_{1-x})_{16}Ge_{30}$ with $x = 0$ and 0.25. a) 2θ from 20° to 60° and b) 2θ from 28° to 32°.

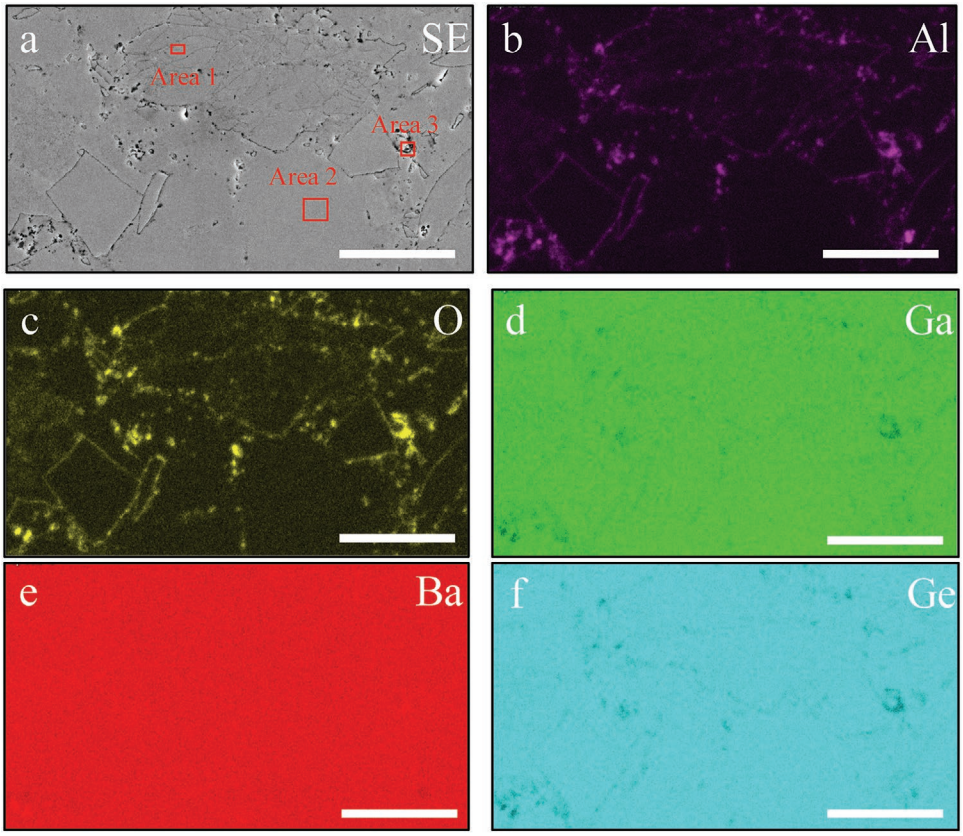

Figure 6. SEM analysis of SPS sintered sample $Ba_8(Al_{0.25}Ga_{0.75})_{16}Ge_{30}$ showing a) secondary electron (SE) micrograph, and b–f) elemental distribution maps of b) Al, c) O, d) Ga, e) Ba, and f) Ge. The average compositions of the selected areas measured by EDX are $Ba_8Al_{2.9}Ga_{12.2}Ge_{28.2}$ (area 1), $Ba_8Al_{2.4}Ga_{12.1}Ge_{28.4}$ (area 2) and $Ba_8Al_{19.5}Ga_{7.8}Ge_{17.3}O_{37.2}$ (area 3), respectively. The corresponding spectra are included in the supporting information. Scale bar is 25 µm.

The reduction of the lattice thermal conductivity is even more pronounced for sample $x = 0.25$, where κ_l is extremely low and remains unchanged from 100–300 °C.

The significant decrease in thermal conductivity is most likely due to enhanced phonon scattering through two mechanisms: atomic-scale disorder as well as the presence of mesoscale grains with varying composition and size. The former refers to the fact that the substitution of Ga with Al induces mass fluctuation scattering in the host structure while the latter is caused by the Al particles/inclusions, which can also scatter heat-carrying phonons. Even so, we do not aim to scrutinize the effect of alloying on the thermal conductivity in the present study because the rattling mode of the Ba atoms might also be affected by changes in the composition of the host structure.[33,34]

To further elucidate the thermal properties of these materials, the specific heat capacity of sample $Ba_8(Al_{0.25}Ga_{0.75})_{16}Ge_{30}$ was measured. The results, which are presented in Figure 8c, show that there exists a weak linear dependence below 400 °C and a sharper slope above 400 °C. For comparison, the specific heat capacity of polycrystalline $Ba_8Ga_{16}Ge_{30}$ exhibits a slightly different behavior: it rises steadily below 350 °C, undergoes an abrupt increase around 400 °C, to a value of about 0.361 J g^{-1} K^{-1}, before plateauing out.[8] The difference is that the C_p previously reported for $Ba_8Ga_{16}Ge_{30}$ samples remains constant after the transition, while that of our $Ba_8(Al_{0.25}Ga_{0.75})_{16}Ge_{30}$ continues to increase. Considering that the microstructure of our sample is not a homogeneous single phase, it is difficult to explain this behavior in the present study.

2.4. Figure of Merit *zT*

The values of zT for the $Ba_8(Al_xGa_{1-x})_{16}Ge_{30}$ materials were calculated and are shown in Figure 8d. The zT for $Ba_8Ga_{16}Ge_{30}$ reaches a maximum value of 0.69 at 550 °C, similar to pressed powders of $Ba_8Ga_{16}Ge_{30}$ reported previously.[8] With the introduction of $Ba_8Al_{16}Ge_{30}$, sample $x = 0.20$ exhibits a maximum zT of 0.67 at 600–650 °C, which decreases at higher temperatures. The optimal zT is achieved for sample $x = 0.25$, with a value of 0.93 at 800 °C. Unfortunately, the thermal conductivity of sample $x = 0.23$ could not be measured due to the small size. If it is assumed that $x = 0.23$ has the same thermal conductivity as sample $x = 0.25$, then the zT of the former would reach 0.99 at 800 °C.

3. Conclusion

The thermoelectric performance of $Ba_8Ga_{16}Ge_{30}$ has been improved through modulation doping, achieved by alloying

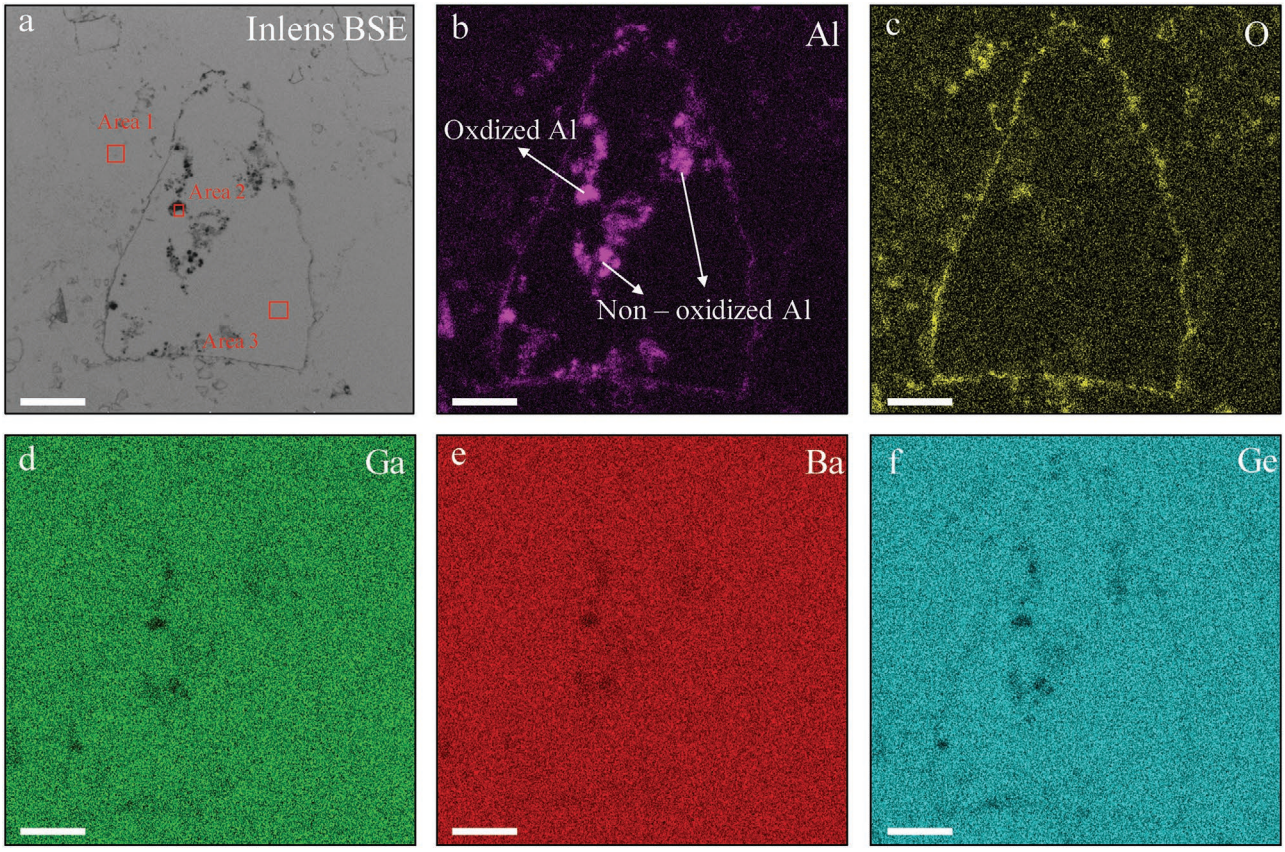

Figure 7. SEM analysis of a clathrate grain in the SPS sintered sample $Ba_8(Al_{0.25}Ga_{0.75})_{16}Ge_{30}$ showing a) in-lens backscattered electron (BSE) micrograph, and b–f) elemental distribution maps of b) Al, c) O, d) Ga, e) Ba, and f) Ge. The average compositions of the selected areas measured by EDX are $Ba_8Al_{2.9}Ga_{11.3}Ge_{28.0}$ (area 1), $Ba_8Al_{77.2}Ga_{8.1}Ge_{23.3}O_{29.8}$ (area 2) and $Ba_8Al_{2.8}Ga_{11.9}Ge_{27.9}$ (area 3), respectively. The corresponding spectra are included in the supporting information. Scale bar is 10 μm.

25 at% $Ba_8Al_{16}Ge_{30}$ with 75 at% $Ba_8Ga_{16}Ge_{30}$, which results in a significantly higher charge carrier mobility, exceeding that of a single crystal with the same composition. This yields an improved electrical conductivity without decreasing the Seebeck coefficient, producing the highest reported power factor among sintered type-I clathrate compounds. Microscopy reveals that the material is composed of a Ga-rich clathrate matrix phase, and Al particles/inclusions, which aggregate on the grain boundaries and inside the grains. Moreover, the lattice thermal conductivity is significantly reduced, which can be attributed to alloy scattering as well as the microstructure. As a result, the highest zT is achieved for samples $x = 0.23$ and 0.25 with values of 0.99 and 0.93, respectively, at 800 °C.

We have proved that modulation doping can be utilized in clathrate compounds, by introducing an analogous compound to the matrix phase. It could be even more beneficial to use this methodology for other systems characterized by a larger Seebeck coefficient and a poorer electrical conductivity.

4. Experimental Section

Material Synthesis: Barium (crystalline dendritic solid, Alfa Aesar, 99.9 %), gallium (metallic liquid, Sigma-Aldrich, 99.9995 %), aluminum (beads, Sigma-Aldrich, 99.9 %), germanium (chips, Sigma-Aldrich, 99.999 %) were used in the synthesis. Polycrystalline $Ba_8Ga_{16}Ge_{30}$ was synthesized according to a previous method.[35] Polycrystalline $Ba_8Al_{16}Ge_{30}$ was made in a similar way: the elements were mixed in an alumina crucible inside an argon-filled glovebox and transferred to a horizontal tube furnace, heated to 1090 °C, dwelled for 2 h and then cooled to 850 °C in 30 h. After annealing at 850 °C for 30 h, the product was cooled to room temperature in 10 h. After the reaction, both $Ba_8Ga_{16}Ge_{30}$ and $Ba_8Al_{16}Ge_{30}$ were washed with concentrated hydrochloric acid, ethanol and water, and finally dried in air.

Sample Preparation: To prepare dense pellets of the clathrates, the material was ground with the help of a ball mill (Mixer Mill MM400, Retsch), before being compacted using a spark plasma sintering (SPS) machine (Dr. Sinter 5.4, SPS Syntex Inc., Japan). The powderized material was placed in a graphite die-punch setup, with an inner diameter of 20.5 mm. Graphite paper was inserted between die and punches, as well as between the material and the punches. The SPS chamber was evacuated, the pressure preset to 75 MPa and then the material was first heated to 700 °C in 4 min, which was followed by a 5 min dwell before being heated to 800 °C where it was held for 15 min. Thereafter the current was turned off, the pressure released, and the temperature lowered to room temperature. The pellets thus obtained were 4–5 mm in thickness. They were polished until no graphite paper remained on the surface. The density of the pellets was determined by the Archimedes method.

Structure and Composition Analysis: Powder X-ray diffraction (XRD) was performed using a Bruker XRD D8 Advance with monochromatic Cu Kα1 radiation. Samples were ground by mortar and pestle. Data were collected using a 1 h scan with 2θ angles from 20° to 60° and plotted, in Figure 5, without normalization.

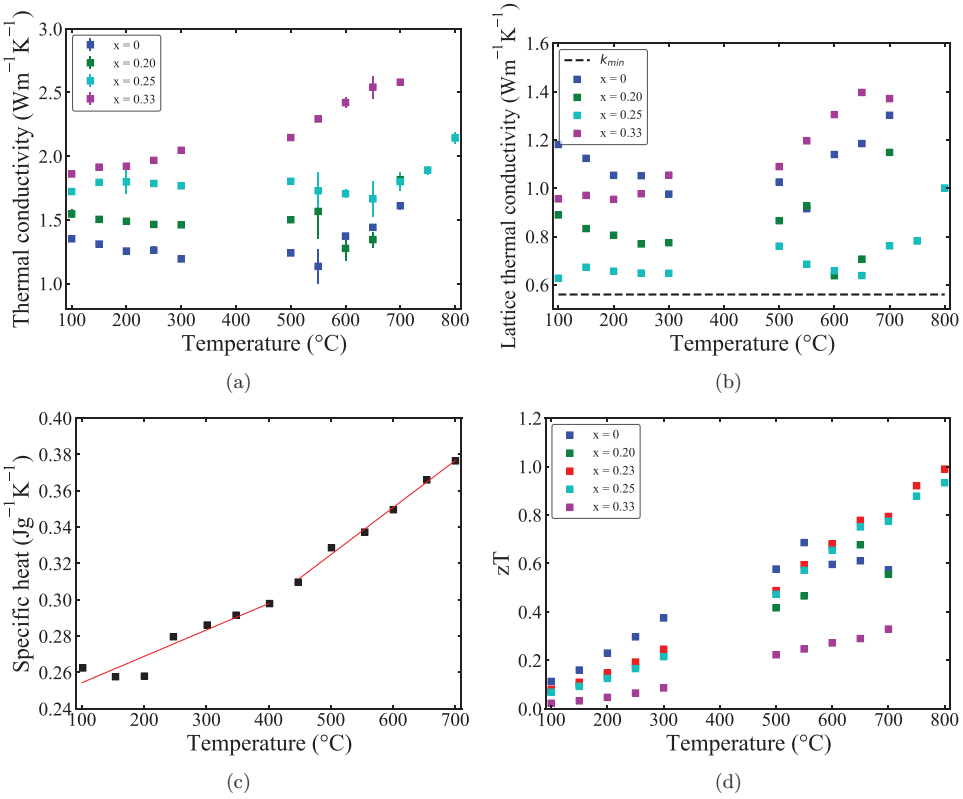

Figure 8. a) Thermal conductivity and b) lattice thermal conductivity of $Ba_8(Al_xGa_{1-x})_{16}Ge_{30}$, x = 0, 0.20, 0.25 and 0.33). κ_{min} refers to the theoretical minimum lattice thermal conductivity of $Ba_8Ga_{16}Ge_{30}$.[8] c) Measured specific heat capacity of the SPS sintered sample $Ba_8(Al_{0.25}Ga_{0.75})_{16}Ge_{30}$, in which the two red lines represent linear fits to the data. d) The figure of merit zT of SPS sintered $Ba_8(Al_xGa_{1-x})_{16}Ge_{30}$, where the zT of sample x = 0.23 is calculated by assuming that it has the same lattice thermal conductivity as sample x = 0.25.

Sintered samples were mechanically polished with SiC sandpaper and diamond spray before microscopy analysis. An Ultra 55 FEG SEM equipped with an Oxford INCA EDX system was used to characterize the sample $Ba_8(Al_{0.50}Ga_{0.50})_{16}Ge_{30}$.

Sample $Ba_8(Al_{0.25}Ga_{0.75})_{16}Ge_{30}$ was, additionally, characterized using a Tescan GAIA3 instrument that integrates a scanning electron microscope (SEM) with a focused ion beam (FIB). The electron beam was accelerated with a high voltage of 20 kV. SEM imaging was performed with in-lens backscattered electron (BSE) and secondary electron (SE) detectors. The chemical composition analysis was done via X-ray energy dispersive spectrometry (EDX), and the EDX signals were collected using an Oxford X-MAX 80 mm^{-2} detector.

Electrical Transport Property Measurements: The electrical resistivity and Seebeck coefficient were measured from 100 to 700 °C using a ZEM-3 (ULVAC) instrument under low pressure in a He atmosphere. Samples were cut to rod-like shapes, with sizes of about 2 × 2 × 8 mm^{-3}, with help of a diamond saw (Struers). Graphite sheets (Goodfellow Cambridge Ltd.) were inserted between the sample and the platinum electrodes of the instrument, in order to avoid reactions between the two.

Specific Heat Capacity Measurements: Specific heat capacity measurements were performed on sample $Ba_8(Al_{0.25}Ga_{0.75})_{16}Ge_{30}$ with a thermal gravimetry analysis (TGA) instrument (Mettler Toledo TGA/DSC3+) using the sapphire method (E1269 - 11). The sample was placed inside a 70 µL platinum crucible, and a piece of graphite paper was inserted between the sample and the crucible. It was heated to 750 °C under a N_2 atmosphere with a heating rate of 20 K min^{-1}, and the specific heat (C_p) was calculated based on the second heating curve.

Thermal Conductivity Measurements: The Hot Disk method (instrument model TPS 3500) was used to measure the thermal conductivity.[36] The mica sensor 5465 was used for the high-temperature measurement. The samples were divided into two discs, and the sensor was tightly sandwiched between them. The thermal conductivity measurement was performed from 100–700 °C under a helium atmosphere, but data could not be acquired in the interval 350 °C–450 °C because the probe is made up of a Ni spiral (which has a Curie temperature of 358 °C). Sample $Ba_8(Al_{0.25}Ga_{0.75})_{16}Ge_{30}$ was further measured up to 800 °C. The heating power was 200–300 mW and the measurement time was 2 s. The measurement at each temperature was repeated five times and the presented results represent an average over the five measurements.

Supporting Information

Supporting Information is available from the Wiley Online Library or from the author.

Acknowledgements

The authors gratefully acknowledge funding for this study from the Swedish Foundation for Strategic Research (SSF) through the Swedish national graduate school in neutron scattering (SwedNess) as well as the Danish Council for Strategic Research via the Programme Commission on Sustainable Energy and Environment through sponsoring of the project "CTEC - Center for Thermoelectric Energy Conversion" (project no. 1305-00002B).

Conflict of Interest

The authors declare no conflict of interest.

Keywords

clathrates, heterostructures, modulation doping, thermoelectrics

Received: July 30, 2020
Revised: November 5, 2020
Published online:

[1] J. He, T. M. Tritt, *Science* **2017**, *357*, 6358.
[2] D. Beretta, N. Neophytou, J. M. Hodges, M. G. Kanatzidis, D. Narducci, M. Martin-Gonzalez, M. Beekman, B. Balke, G. Cerretti, W. Tremel, A. Zevalkink, A. I. Hofmann, C. Muller, B. Dorling, M. Campoy-Quiles, M. Caironi, *Mater. Sci. Eng., R* **2019**, *138*, 210.
[3] G. J. Snyder, E. S. Toberer, *Nat. Mater.* **2008**, *7*, 105.
[4] Y. Ma, R. Heijl, A. E. C. Palmqvist, *J. Mater. Sci.* **2012**, *48*, 2767.
[5] D. M. Rowe, *CRC Handbook of Thermoelectrics*, CRC Press, Boca Raton, FL **1995**.
[6] J. A. Dolyniuk, B. Owens-Baird, J. Wang, J. V. Zaikina, K. Kovnir, *Mater. Sci. Eng., R* **2016**, *108*, 1.
[7] A. Saramat, G. Svensson, A. E. C. Palmqvist, C. Stiewe, E. Mueller, D. Platzek, S. G. K. Williams, D. M. Rowe, J. D. Bryan, G. D. Stucky, *J. Appl. Phys.* **2006**, *99*, 023708.
[8] A. F. May, E. S. Toberer, A. Saramat, G. J. Snyder, *Phys. Rev. B* **2009**, *80*, 12.
[9] N. Neophytou, M. Thesberg, *J. Comput. Electron.* **2016**, *15*, 16.
[10] J. P. Heremans, V. Jovovic, E. S. Toberer, A. Saramat, K. Kurosaki, A. Charoenphakdee, S. Yamanaka, G. J. Snyder, *Science* **2008**, *321*, 554.
[11] Y. Z. Pei, X. Y. Shi, A. LaLonde, H. Wang, L. D. Chen, G. J. Snyder, *Nature* **2011**, *473*, 66.
[12] M. Zebarjadi, G. Joshi, G. Zhu, B. Yu, A. Minnich, Y. Lan, X. Wang, M. Dresselhaus, Z. Ren, G. Chen, *Nano Lett.* **2011**, *11*, 2225.
[13] D. Wu, Y. Pei, Z. Wang, H. Wu, L. Huang, L.-D. Zhao, J. He, *Adv. Funct. Mater.* **2014**, *24*, 7763.
[14] Y.-L. Pei, H. Wu, D. Wu, F. Zheng, J. He, *J. Am. Chem. Soc.* **2014**, *136*, 13902.
[15] S. A. Yamini, D. R. G. Mitchell, Z. M. Gibbs, R. Santos, V. Patterson, S. Li, Y. Z. Pei, S. X. Dou, G. Jeffrey Snyder, *Adv. Energy Mater.* **2015**, *5*, 21.
[16] J. Wang, B.-Y. Zhang, H.-J. Kang, Y. Li, X. Yaer, J.-F. Li, Q. Tan, S. Zhang, G.-H. Fan, C.-Y. Liu, L. Miao, D. Nan, T.-M. Wang, L.-D. Zhao, *Nano Energy* **2017**, *35*, 387.
[17] N. Melnychenko-Koblyuk, A. Grytsiv, P. Rogl, M. Rotter, R. Lackner, E. Bauer, L. Fornasari, F. Marabelli, G. Giester, *Phys. Rev. B* **2007**, *76*, 19.
[18] J. Wang, O. I. Lebedev, K. Lee, J. A. Dolyniuk, P. Klavins, S. Bux, K. Kovnir, *Chem. Sci.* **2017**, *8*, 8030.
[19] D. Cederkrantz, M. Nygren, A. E. C. Palmqvist, *J. Appl. Phys.* **2010**, *108*, 11.
[20] X. Yan, M. Ikeda, L. Zhang, E. Bauer, P. Rogl, G. Giester, A. Prokofiev, S. Paschen, *J. Mater. Chem. A* **2018**, *6*, 1727.
[21] X. Shi, J. Yang, S. Q. Bai, J. H. Yang, H. Wang, M. F. Chi, J. R. Salvador, W. Q. Zhang, L. D. Chen, W. Wong-Ng, *Adv. Funct. Mater.* **2010**, *20*, 755.
[22] M. Christensen, B. B. Iversen, *Chem. Mater.* **2007**, *19*, 4896.
[23] T. Uemura, K. Akai, K. Koga, T. Tanaka, H. Kurisu, S. Yamamoto, K. Kishimoto, T. Koyanagi, M. Matsuura, *J. Appl. Phys.* **2008**, *104*, 1.
[24] G. J. Snyder, A. H. Snyder, M. Wood, R. Gurunathan, B. H. Snyder, C. Niu, *Adv. Mater.* **2020**, *32*, 2001537.
[25] H. H. Xie, H. Wang, C. G. Fu, Y. T. Liu, G. J. Snyder, X. B. Zhao, T. J. Zhu, *Sci. Rep.* **2014**, *4*.
[26] M. Christensen, S. Johnsen, B. B. Iversen, *Dalton Trans.* **2010**, *39*, 978.
[27] E. S. Toberer, M. Christensen, B. B. Iversen, G. J. Snyder, *Phys. Rev. B* **2008**, *77*, 7.
[28] A. Prokofiev, A. Sidorenko, K. Hradil, M. Ikeda, R. Svagera, M. Waas, H. Winkler, K. Neumaier, S. Paschen, *Nat. Mater.* **2013**, *12*, 1096.
[29] Y.-H. Hou, L.-S. Chang, *J. Alloys Compd.* **2018**, *736*, 108.
[30] K. Biswas, J. He, I. D. Blum, C.-I. Wu, T. P. Hogan, D. N. Seidman, V. P. Dravid, M. G. Kanatzidis, *Nature* **2012**, *489*, 414.
[31] M. Christensen, G. Snyder, B. Iversen, in *Int. Conf. on Thermoelectrics*, IEEE, Piscataway, NJ **2006**, pp. 40–43.
[32] H. S. Kim, Z. M. Gibbs, Y. L. Tang, H. Wang, G. J. Snyder, *APL Mater.* **2015**, *3*, 4.
[33] M. Ångqvist, P. Erhart, *Chem. Mater.* **2017**, *29*, 7554.
[34] D. O. Lindroth, J. Brorsson, E. Fransson, F. Eriksson, A. Palmqvist, P. Erhart, *Phys. Rev. B* **2019**, *100*, 4.
[35] R. Heijl, D. Cederkrantz, M. Nygren, A. E. C. Palmqvist, *J. Appl. Phys.* **2012**, *112*, 044313.
[36] S. E. Gustafsson, *Rev. Sci. Instrum.* **1991**, *62*, 797.